Journal of
Materials Chemistry A

Materials for energy and sustainability

Accepted Manuscript

This article can be cited before page numbers have been issued, to do this please use: H. Luo, X. Xie, J. Sun, S. Guo and I. Khalakhan, *J. Mater. Chem. A*, 2026, DOI: 10.1039/D5TA07392H.

ROYAL SOCIETY OF CHEMISTRY

rsc.li/materials-a

View Article Online
DOI: 10.1039/D5TA07392H

COMMUNICATION

Effective and Selective Ethylene Glycol Electrooxidation with Compositionally Controlled Pt-Au Bimetallic Electrocatalysts

Hui Luo,*[a] Xianxian Xie,[b] Jiamin Sun,[c] Shaohui Guo,[c] Ivan Khalakhan*[b]

Received 00th January 20xx,
Accepted 00th January 20xx

DOI: 10.1039/x0xx00000x

Controlling surface Pt and Au concentration on PtAu nanoparticles via magnetron sputtering enables enhanced EGOR activity and glycolate selectivity. This improvement originates from structural modifications of Pt induced by adjacent Au atoms, inducing electronic and strain effects. These findings highlight surface composition engineering as a promising strategy for designing next-generation nanoparticle electrocatalysts with tailored performance.

Introduction

Polyethylene terephthalate (PET), made from repeat monomer units of terephthalic acid (TPA) and ethylene glycol (EG), is a widely used plastic product. In 2019, consumption of PET reached 710 kton in the UK only and accounted for 27% of all plastic types.[1] Although 44.2% were recycled through mechanical recycling processes,[2] they cannot be recycled this way infinitely, as the material degrades over time and becomes unsuitable for producing food-grade containers. Therefore, the end-of-life PET currently ends up in landfills or incineration facilities, while market demand for virgin PET still exceeds 600 kton/year.[3] In this regard, recent research has focused on chemical recycling which can recover the pure monomer TPA from the end-of-life PET for virgin PET manufacturing.[4–7] However, the by-product, ethylene glycol (EG) that contains contaminants from the waste stream, is miscible with water with high boiling point. Therefore, it is hard to separate out and has low economic value. It is crucial to also upcycle this by-product and generate additional benefits to promote the recycling rate. In this regard, the electrochemical ethylene glycol oxidation reaction (EGOR) to coproduce green H_2 and value-added chemicals at low potential constitutes a promising strategy. On this aspect, the market for EG oxidation product glycolic acid has grown significantly, as it is a valuable commodity chemical but conventionally produced via petrochemistry, with applications in bio-polymer and cosmetic products and a market value reaching $531.5 million by 2027. Combining the production of green H_2 and glycolic acid, this approach would lead to an overall better economic and environmental impact. As a result, there is an increasing number of research on EGOR in recent years.[8,9]

In general, a good EGOR catalyst should be able to activate the EG molecule at a relatively negative potential and have fast kinetics to reach high current density. At the same time, it should also exhibit high selectivity towards desired anodic chemical products, e.g. glycolic acid. Pt-based electrocatalysts are the state-of-the-art for EG electrooxidation. Pt surface can adsorb EG molecules effectively and catalyse C-H, C-O, C-C bond cleavage. However, because of the same reason, Pt also suffers from deactivation due to overoxidation and poisoning from formic acid and CO-like intermediates.[10,11] Therefore, moving forward, it is important to modulate the Pt catalyst structure to achieve and balance high activity, high selectivity towards glycolic acid, and high poison-tolerance.

In recent studies, attention has been paid to using Pt-Au bimetallic electrocatalysts for alcohol oxidation due to Au's high chemical stability and better poison tolerance. For example, Shao-Horn and co-workers found that surrounding surface Au atoms can effectively weaken CO binding on Pt in discrete Pt or Pt-rich clusters, thus enhancing activity towards CO and methanol oxidation.[12] Dai et al. prepared a series of AuPt nanoparticles for electrochemical glycerol-to-lactic acid conversion, and showed that with an Au-enriched surface, the lactic acid selectivity can reach 73% at 0.45 V_{RHE}.[13] Although the authors did not investigate in detail the role of Au in tuning the product selectivity, such results clearly show the benefit of alloying Au in altering the reaction pathway. More recently, Li et

[a] School of Engineering, Stag Hill Campus, University of Surrey, Guildford, UK, GU2 7XH.
[b] Department of Surface and Plasma Science, Faculty of Mathematics and Physics, Charles University, V Holešovičkách 2, 18000 Prague 8, Czech Republic.
[c] College of Chemistry and Chemical Engineering, Taiyuan University of Technology, 030024, Taiyuan, Shanxi, China.

† Supplementary Information available: [Experimental section, material characterisation, extra electrochemical results]. See DOI: 10.1039/x0xx00000x

al. designed a PtAu alloy catalyst on Ni foam (hp-PtAu/NF) for glycerol electrooxidation, which showed that the introduction of Au can significantly facilitate the adsorption of hydroxyl species, thus improving glycerol oxidation activity. [14]

However, so far there are limited studies of PtAu on EGOR, especially those using structurally uniform and compositionally fine-tuned systems,[15,16] Herein, we present a systematic study of EGOR on Pt-Au bimetallic electrocatalysts with different Pt to Au ratios. By tuning the surface composition of Pt-Au, we aim to establish the correlation between surface composition and catalytic performance for EGOR ($C_2H_6O_2 + H_2O \rightarrow C_2H_4O_3 + 2H_2$), and provide preliminary insights on the influence of electronic structure changes within the PtAu electrodes.

Results and Discussion

A series of Pt-Au bimetallic alloys with the same thickness of 10 nm but different compositions were prepared using a magnetron co-sputtering technique (**Figure 1a**), referred to as PtAu5, PtAu10 and PtAu20, corresponding to $Pt_{95}Au_5$, $Pt_{90}Au_{10}$ and $Pt_{80}Au_{20}$, respectively. These samples are prepared using the identical parameters as in our previous work.[17] In addition, pure Pt and Au electrodes were also fabricated using the single targets as control samples.

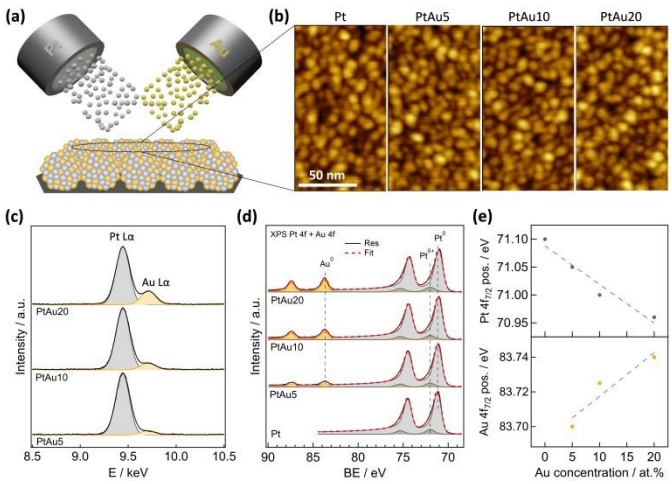

Figure 1. (a) Illustration of the magnetron sputtering deposition process, (b) AFM images of the as-deposited pure Pt and Pt–Au alloy catalysts, (c) EDX and (b) XPS spectra acquired for as-deposited Pt–Au alloy catalysts and pure Pt, (e) Pt $4f_{7/2}$ and Au $4f_{7/2}$ peaks position extracted from the XPS spectra shown in (d).

The morphology of the as-deposited layers was examined by atomic force microscopy (AFM). As shown in **Figure 1b**, all catalysts exhibit homogeneously distributed grains, characteristic of sputter-deposited thin films,[18] with nearly identical morphologies, indicating that morphology will not impact further catalytic activity measurements. The composition of the samples was characterized using bulk-sensitive energy-dispersive X-ray spectroscopy (EDX) and surface-sensitive X-ray photoelectron spectroscopy (XPS) techniques. **Figure 1c** displays the Pt Lα and Au Lα EDX spectra, while **Figure 1d** shows the Pt 4f and Au 4f XPS spectra, used for quantitative analysis. The corresponding survey spectra are provided in **Figure S1**. The EDX spectra of the as-deposited Pt-Au alloys were deconvoluted into two peaks at 9.44 and 9.71 keV, assigned to Pt Lα and Au Lα, respectively. The XPS core levels exhibit three doublets at about 84.0/87.7, 71.1/74.4, and 72.0/75.3 eV, attributed to Au^0, Pt^0 and $Pt^{\delta+}$ states, respectively.[17,19,20] The presence of a small fraction of $Pt^{\delta+}$ states could be related to adsorbate-induced partial surface oxidation of platinum during samples transferring through air.[20] A closer look at the XPS spectra reveals a continuous shift of the Pt 4f and Au 4f regions (highlighted in Figure 1d as Pt $4f_{7/2}$ and Au $4f_{7/2}$ position) with increasing Au concentration in the alloy, indicating changes in electronic structure of both Pt and Au due to alloying. A more comprehensive characterization of identically prepared Pt-Au samples, including CO stripping, synchrotron radiation photoelectron spectroscopy and X-ray diffraction, can be found in our previous work, which demonstrates the precise adjustment of the amount of gold in Pt-Au alloy allows accurate tuning of platinum geometrical and electronic structure.[17] Quantitative analysis of the EDX and XPS spectra reveals nearly identical Pt-Au catalyst compositions (see **Table S1**), confirming that the Au content on the surface matches that in the bulk. This indicates a homogeneous Pt-Au atomic ratio across the deposited layers, consistent with our earlier study.

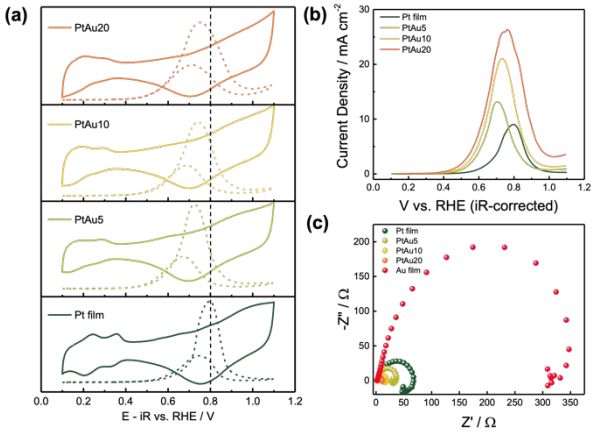

Figure 2. Electrochemical EGOR activity of the PtAu and Pt electrodes. (a) CV profiles in 1 M NaOH with/without 0.1 M EG, scan rate: 50 mV s^{-1}. (b) LSV profiles in 0.1 M EG + 1 M NaOH, scan rate: 10 mV s^{-1}. (c) EIS Nyquist plot in 0.1 M EG + 1 M NaOH at 0.7 V_{RHE}, frequency: 100 kHz to 0.1 Hz.

Given that the thin film electrodes possess homogenous PtAu ratio, flat surface and fine-tuned composition, they are ideal in conducting fundamental study for EGOR, as factors such as surface roughness caused mass transport differences, composition inhomogenicity across different catalysts are largely limited. However, we have to point out that electrodes with such thin film configuration tend to be instable due to delamination between the thin film and substrate, and therefore cannot be used in longer term stability measurements. Herein, the electrochemical activity of all the film electrodes was first evaluated in 1 M NaOH with and without 0.1M EG addition in three-electrode configurations. Comparing the cyclic voltammetry (CV)

View Article Online
DOI: 10.1039/D5TA07392H

(**Figure 2a**) and linear sweep voltammetry (LSV) (**Figure 2b**) profiles in the presence of EG, it can be seen that increasing the surface Au concentration enhanced the intrinsic activity of EGOR compared with pure Pt, with the starting potential negatively shifted to lower potential. The current density at the peak potentials also follows the trend of PtAu20 > PtAu10 > PtAu5 > Pt. We hypothesize the enhancement in the EGOR kinetics of PtAu catalysts to stem from the modified electronic structure of surface Pt that is surrounded by Au neighbors, which results in a weakened binding strength of carbon-based intermediate species. This hypothesis is supported by previous studies on single-crystal with similar Pt rich surface configuration, which has shown to have weaker CO binding contribution from the next nearest Au atoms.[21,22] However, since the alloying with Au has also induced tensile strain in the electrode originating from the larger Au atom, as evidenced from the XRD results in our previous work,[17] we can not rule out the role of strain effect in controlling the PtAu electrodes' EGOR activity. In bimetallic systems, these electronic and geometric effects always occur simultaneously, influencing the catalytic properties together. As a result, it is challenging to isolate the contribution of each effect experimentally or theoretically, and the observed changes in activity or stability are typically a combination of both factors.[23]

We then extended the potential range to observe distinctive features related to surface activities on Au sites. As shown in **Figure S2**, after alloying with Au, redox peaks associated with Au oxidation and reduction can be observed at near 1.2 V_{RHE} and 1V_{RHE}, respectively, indicating the presence of Au at the electrochemical interface. Such peaks became more pronounced with higher Au loading, further validates the material characterization results. It can be noticed that a tiny EG oxidation peak attributed to EG oxidation on Au (**Figure S3**) can be observed near 1.1 V_{RHE}, which potential remains unchanged. Such results suggest that the reactivity of Au sites in the PtAu electrodes remains constant, and the increased EGOR activity is attributed mainly to the Pt sites that are affected by the nearby Au atoms,[24] in line with the hypothesis above. To gain more understanding of how surface Au enhances the EGOR performance of Pt sites, we then performed electrochemical EIS measurements in the presence of EG. As shown in **Figure 2c**, among all the electrodes, PtAu20 exhibits the smallest semi-circle, suggesting the lowest charge transfer resistance at the electrochemical interface. Such improved interfacial charge transfer process enables fast, concerted proton-coupled electron transfer during EGOR, improve the reaction kinetics and thus lower the overpotential, as seen in Figure 2b. Next, we took a closer look at the CVs of all Pt-based electrodes in the 1M NaOH supporting electrolyte shown in **Figure S4**. In the potential region of 0.4 – 0.7 V_{RHE}, where *OH adsorption taking place on Pt sites, PtAu5 and PtAu10 exhibited a peak at ~0.6 V_{RHE}, with slightly higher current density and a shift towards more negative potential. In contrast, the PtAu20 electrode showed a decreased current density in this region than Pt electrode. It is well-known that surface adsorbed *OH is a key reactant for EG oxidation.[25] Therefore, although higher Au loading has led to lower charge transfer resistance, an excess amount of Au may hinder the *OH adsorption on Pt sites, as unlike Ru or Sn, Au is much more inert.[12] These competing factors determine that there's an optimal Pt-Au composition for EGOR.

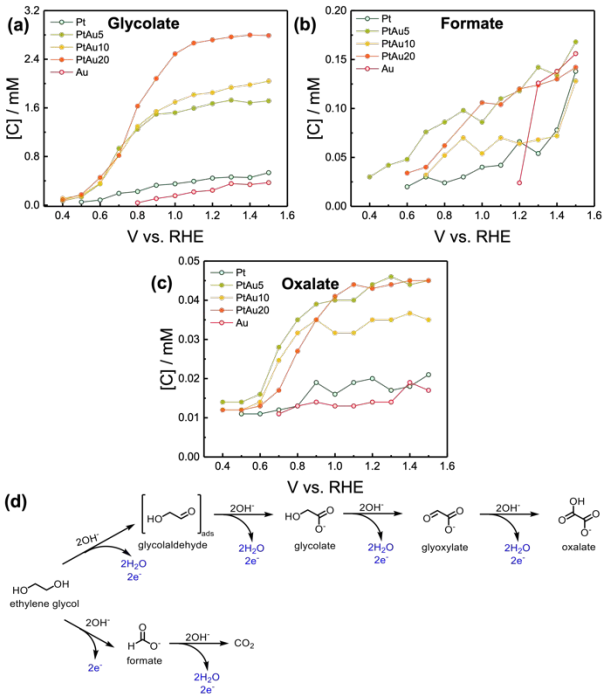

Figure 3. EGOR product concentration as a function of potential on different electrodes analysed by HPLC: (a) glycolate, (b) formate, (c) oxalate. The corresponding chronoamperometry profiles are included in **Figure S5**. (d) proposed reaction pathway.

Subsequently, we investigated the product selectivity as a function of applied potential by performing chronoamperometry measurements. The instantaneous oxidation products at different potentials were analysed by high-performance liquid chromatography (HPLC) using the calibration curve shown in **Figure S6**. Given the low concentration of the generated products, we have calibrated the instrument to a range within 0.01 – 2.5 mM. As shown in **Figure 3a-c** and **Figure S7**, on all electrodes, only glycolate (salt form of glycolic acid), oxalate (salt form of oxalic acid) and formate (salt form of formic acid) were detected as the stable products in liquid electrolyte, which can represent the products distribution in the EGOR system. It should be noted that carbonate may also be formed as an over-oxidation product of EG, but its presence cannot be detected by HPLC. The first observed product, glycolate, was detected since 0.4 V_{RHE} among all electrodes containing Pt (PtAu5, PtAu10, PtAu20, Pt), while with Au electrode it is only until 0.8V_{RHE} when the product started to appear, in good agreement with the observed starting potential seen in CV and LSV measurements as well as previous study.[10,26] Specifically, the glycolate concentration in PtAu electrodes is much higher than that of Pt and Au electrodes. On the contrary, the minor product formate concentration appeared to be in a similar range among all film electrodes, suggesting that the enhanced electrochemical activities were originated from the EG to glycolate conversion. According to Li et al., such change in product selectivity could be attributed to the optimized adsorption geometry of alcohol molecule on the catalyst surface. Rather than binding

through two C atoms, the Pt-Au surface favors the binding configuration of one terminal C atom, which effectively prevents the C-C bond breaking into formate.[14] Furthermore, the alloying with Au may also facilitated glycolate desorption from the catalyst surface, preventing the over-oxidation towards oxalate and formate.

Different from the Pt-based electrodes, on Au film, formate product was not detected until 1.2 V_{RHE}, 400 mV more positive than glycolate. The formate concentration also increased rapidly at higher potential compared to that of the Pt-based electrodes. Such potential (> 1.2 V_{RHE}) is related to the surface Au oxidation formation as seen in **Figure S2** and previous reports,[25] which may suggest that as the Au oxidation state changes, the EG oxidation pathway shifts towards promoting C-C cleavage.

Electrochemical *in situ* Raman spectroscopy was employed to further intuitively clarify dynamic changes in the PtAu20 electrode during the EGOR process in 1 M NaOH with 0.1 M EG addition at various potentials. **Figure S8** shows strong peaks at around 490 cm^{-1}, corresponding to Pt-C stretching mode.[27] The peaks at 603 cm^{-1} and 798 cm^{-1} are assigned to the bending mode of δ (Pt-O)[28] and δ (Au-O),[29,30] respectively. The bands around 1055 cm^{-1} and 1083 cm^{-1}, which can be assigned to the intermediate bonded with the carbon atoms of EG,[30] remain unchanged over the studied potential range. This phenomenon can be due to different reasons. First, EG adsorption on the PtAu20 surface is in excess, in which the signals from the reacted molecules cannot be distinguished. Secondly, as EG is a strong adsorbing molecule like glycerol on Pt surface, certain reacted species may not desorb, especially at higher potentials where the adsorption energy is higher. Finally, despite the presence of Au enabling a surface enhanced Raman effect, the signals may still be disturbed by the bulk electrolyte, and therefore the subtle features from the surface interface are over-shadowed. Therefore, no qualitative results are derived from *in situ* Raman study, and further studies, such as roughing the surface for stronger surface enhancement, are required for future work.

Conclusions

In summary, we show that controlling the surface atomic concentration of Au on PtAu nanoparticles is critical for enhancing the EGOR activity. By fine-tuning the surface Au composition using magnetron sputtering, both the catalytic activity and selectivity towards glycolate can be enhanced. We hypothesis that such enhancement in the EGOR kinetics of PtAu catalysts is stemed from the modified electronic structure of surface Pt that is surrounded by Au neighbors, and future work will focus on mechanistic investigations to correlate the surface composition-electronic structure-electrochemical performance. Our work demonstrates that electronic structure control by way of surface composition manipulation represents another avenue for designing a future generation of nanoparticle electrocatalysts.

Conflicts of interest

There are no conflicts to declare.

Data availability

View Article Online
DOI: 10.1039/D5TA07392H

The data supporting this article have been included as part of the Supporting Information. Raw data for this article, including electrochemical testing and liquid product from HPLC, are available at figshare: https://doi.org/10.6084/m9.figshare.30090457.v2.

Acknowledgements

HL acknowledges the support from the Royal Society Research Grant (RG\R1\241164) and the Royal Academy of Engineering Research Fellowship (RF-2324-23-176). This study was completed with the assistance of infrastructure funded by the Ministry of Education, Youth and Sports (MEYS), Czech Republic, through project LM2023072.

References

1 H. Zhou, Y. Ren, Z. Li, M. Xu, Y. Wang, R. Ge, X. Kong, L. Zheng and H. Duan, *Nature Communications 2021 12:1*, 2021, **12**, 1–9.
2 R. Affairs Committee, .
3 Plastic Recycling, https://www.bpf.co.uk/sustainability/plastics_recycling.aspx, (accessed 18 July 2025).
4 A. Singh, N. A. Rorrer, S. R. Nicholson, A. C. Carpenter, J. E. Mcgeehan and G. T. Beckham, DOI:10.1016/j.joule.2021.06.015.
5 Y. Peng, J. Yang, C. Deng, J. Deng, L. Shen and Y. Fu, *Nature Communications 2023 14:1*, 2023, **14**, 1–10.
6 S. Ügdüler, K. M. Van Geem, R. Denolf, M. Roosen, N. Mys, K. Ragaert and S. De Meester, *Green Chemistry*, 2020, **22**, 5376–5394.
7 N. P. Murphy, S. H. Dempsey, J. S. DesVeaux, T. Uekert, A. C. Chang, S. Mailaram, M. Alherech, H. M. Alt, K. J. Ramirez, B. Norton-Baker, E. L. Bell, C. A. Singer, A. R. Pickford, J. E. McGeehan, M. J. Sobkowicz and G. T. Beckham, *Nature Chemical Engineering 2025 2:5*, 2025, **2**, 309–320.
8 H. Luo, J. Barrio, N. Sunny, A. Li, L. Steier, N. Shah, I. E. L. Stephens and M. M. Titirici, *Adv Energy Mater*, DOI:10.1002/AENM.202101180.
9 J. J. Zhao, H. R. Zhu, C. J. Huang, M. H. Yin and G. R. Li, *J Mater Chem A Mater*, 2025, **13**, 3236–3272.
10 L. Xin, Z. Zhang, J. Qi, D. Chadderdon and W. Li, *Appl Catal B*, 2012, **125**, 85–94.
11 Y. Kwon, K. J. P. Schouten and M. T. M. Koper, *ChemCatChem*, 2011, **3**, 1176–1185.
12 J. Suntivich, Z. Xu, C. E. Carlton, J. Kim, B. Han, S. W. Lee, N. Bonnet, N. Marzari, L. F. Allard, H. A. Gasteiger, K. Hamad-Schifferli and Y. Shao-Horn, *J Am Chem Soc*, 2013, **135**, 7985–7991.
13 C. Dai, L. Sun, H. Liao, B. Khezri, R. D. Webster, A. C. Fisher and Z. J. Xu, *J Catal*, 2017, **356**, 14–21.
14 Y. Li, X. Wei, R. Pan, Y. Wang, J. Luo, L. Li, L. Chen and J. Shi, *Energy Environ Sci*, 2024, **17**, 4205–4215.
15 C. Jin, Y. Song and Z. Chen, *Electrochim Acta*, 2009, **54**, 4136–4140.

View Article Online
DOI: 10.1039/D5TA07392H

16 Y. Kim, H. J. Kim, Y. S. Kim, S. M. Choi, M. H. Seo and W. B. Kim, *Journal of Physical Chemistry C*, 2012, **116**, 18093–18100.
17 X. Xie, V. Briega-Martos, R. Farris, M. Dopita, M. Vorokhta, T. Skála, I. Matolínová, K. M. Neyman, S. Cherevko and I. Khalakhan, *ACS Applied Materials and Interfaces* , 2023, **15**, 1192–1200.
18 A. L. M. Sandhya, P. Pleskunov, M. Bogar, X. Xie, P. A. Wieser, M. Orság, T. N. Dinhová, M. Dopita, R. Taccani, H. Amenitsch, A. Choukourov, I. Matolínová and I. Khalakhan, *Surfaces and Interfaces*, 2023, **40**, 103079.
19 X. Xie, V. Briega-Martos, P. Alemany, A. L. Mohandas Sandhya, T. Skála, M. G. Rodríguez, J. Nováková, M. Dopita, M. Vorochta, A. Bruix, S. Cherevko, K. M. Neyman, I. Matolínová and I. Khalakhan, *ACS Catal*, 2025, **15**, 234–245.
20 R. Mom, L. Frevel, J. J. Velasco-Vélez, M. Plodinec, A. Knop-Gericke and R. Schlögl, *J Am Chem Soc*, 2019, **141**, 6537–6544.
21 M. O. Pedersen, S. Helveg, A. Ruban, I. Stensgaard, E. Lægsgaard, J. K. Nørskov and F. Besenbacher, *Surf Sci*, 1999, **426**, 395–409.
22 M. Eyrich, T. Diemant, H. Hartmann, J. Bansmann and R. J. Behm, *Journal of Physical Chemistry C*, 2012, **116**, 11154–11165.
23 C. Lim, A. R. Fairhurst, B. J. Ransom, D. Haering and V. R. Stamenkovic, *ACS Catal*, 2023, **13**, 14874–14893.
24 P. N. Duchesne, Z. Y. Li, C. P. Deming, V. Fung, X. Zhao, J. Yuan, T. Regier, A. Aldalbahi, Z. Almarhoon, S. Chen, D. en Jiang, N. Zheng and P. Zhang, *Nature Materials 2018 17:11*, 2018, **17**, 1033–1039.
25 L. Pérez-Martínez, L. Balke and A. Cuesta, *J Catal*, 2021, **394**, 1–7.
26 Y. Kwon, S. J. Raaijman and M. T. M. Koper, *ChemCatChem*, 2014, **6**, 79–81.
27 S. C. S. Lai, S. E. F. Kleyn, V. Rosca and M. T. M. Koper, *Journal of Physical Chemistry C*, 2008, **112**, 19080–19087.
28 Y. F. Huang, P. J. Kooyman and M. T. M. Koper, *Nat Commun*, 2016, **7**, 1–7.
29 A. Das, B. Mohapatra, V. Kamboj and C. Ranjan, *ChemCatChem*, 2021, **13**, 2053–2063.
30 Y. Li, X. Wei, R. Pan, Y. Wang, J. Luo, L. Li, L. Chen and J. Shi, *Energy Environ Sci*, 2024, **17**, 4205–4215.

Effective and Selective Ethylene Glycol Electrooxidation with Compositionally Controlled Pt-Au Bimetallic Electrocatalysts

View Article Online
DOI: 10.1039/D5TA07392H

Hui Luo,*[a] Xianxian Xie,[b] Jiamin Sun,[c] Shaohui Guo,[c] Ivan Khalakhan*[b]

The data supporting this article have been included as part of the Supporting Information. Raw data for this article, including XPS results, electrochemical testing and liquid product from HPLC, are available at figshare: https://doi.org/10.6084/m9.figshare.30090457.v2